1
Micro-Striplines and Micro-Slot NMR Probes

1.1
Introduction

Nuclear magnetic resonance refers to the interaction of a system of nuclear spins exposed to a static magnetic field with an oscillatory field, usually in the radio frequency range (anywhere from 1 kHz to several GHz) [1]. In the overwhelming majority of cases, the changes in the spin state that result from this interaction are read out through a voltage induced by the spin precession into a surrounding conductor. Even though alternative readout approaches have been demonstrated, and have their advantages in certain cases, this type of inductive detection has proven to be both robust and easy to implement. Indeed, while the earliest demonstrations of nuclear magnetic resonance, pioneered by Rabi,[2] relied on the deflection atomic beams in inhomogeneous fields according to the spin state, NMR did not take off as a widely used tool until the invention of the direct induction method, independently discovered by Bloch[3] and by Purcell, Torrey, and Pound[4] in 1946.

Among other advantages, inductive detection allows the use of the same structure for both excitation and detection of the nuclear spin precession. Particularly in the context of the Fourier spectroscopy method,[5] this has become very useful. It is relatively easy to expose a sample to an oscillatory magnetic field by surrounding it with a suitable conductor, through which an alternating current is sent at the appropriate frequency. The precessing spins induce a measurable voltage in the same conductor. Of course, there are technical problems to be solved that arise due to the high power that is needed in some cases for excitation, while the induced voltages are very small and require exquisitely sensitive receivers. It is not uncommon for excitation RF power to approach several kW, whereas the power available for spin detection is typically of the order of only a few pW.

The earliest inductive NMR systems have almost exclusively relied on solenoid coils as excitation/ detection systems. As the applications of NMR have diversified, and new technologies have become available, other geometries have been explored. In particular, the advent of superconducting magnets with cylindrical bores has led to the development of saddle coils and related resonator geometries. Magnetic resonance imaging, in particular for medical applications, brought the need to

accommodate much larger samples, which was met by the development of birdcage resonators. Hence, most of the current NMR detectors follow a roughly cylindrical form factor. There are some applications, though, which require a more planar geometry. In particular, the study of thin films, membranes, and interfaces is complicated in cylindrical detector systems. Special, flattened solenoid probes have been developed for the study of membrane proteins under solid-state NMR conditions [6]. As the magnetic fields, and, correspondingly, the Larmor frequencies used in MRI scanners have increased, uniform penetration of the radio frequency magnetic fields into the tissue has become more and more difficult. Since biological systems contain ionic solutions, non-conservative electric fields arising in the detector system need to be shielded from getting in contact with the tissue. The dielectric losses incurred from interaction between these electric fields and the tissue degrade the sensitivity of the detection, but they also lead to excessive power deposition in the tissue during excitation. As a solution, surface coils for localised MR imaging of human subjects based on circular or quadratically laid out strip lines have been proposed. [7] NMR spectroscopy is an extremely versatile tool. Nuclear spins turn out to be excellent spies. They are well insulated from the noisy electronic degrees of freedom to allow for long spin coherence life times, which is the basis of sharp spectral lines. At the same time, the nuclear Larmor frequency turns out to depend in subtle ways on the electronic environment. In combination, these two features make it possible to both accurately measure the nuclear Larmor frequency, and to interpret it in terms of the molecular environment that surrounds the nucleus.

Compared to many other spectroscopic techniques, NMR suffers from a major drawback: its relative insensitivity. While UV/VIS techniques, in particular fluorescence, can detect signals from single molecules with relative ease, NMR typically requires of the order of 10^{15} spins to resonate within a narrow bandwidth (1 Hz or so) in order for the signal to be measurable. To some extent, this can be alleviated by long measurement times. Since the signal/noise ratio only grows with the square root of the measurement time, sensitivity still limits the application of NMR in practice. The design of NMR detectors that offer optimal sensitivity has therefore been a long-standing research topic in magnetic resonance. Sensitivity is determined by the signal/noise ratio that can be obtained within a specified amount of time from a defined number of spins. Inductive detectors based on resistive metals invariably produce thermal noise. Under optimal conditions, where all non-intrinsic sources of noise have been eliminated by shielding, the blackbody radiation of the resonator structure itself leads to a noise voltage spectral density which is essentially independent of frequency, and scales proportionally to the square root of the ohmic resistance of the detector. The relationship between the NMR spin precession and the induced voltage signal has been discussed by Hoult and Richards in terms of the correspondence principle.[8] The induced signal strength from a single spin depends on the normalised magnetic field (generated by the detector per unit current) at the location of the spin. Hence, efficient detectors need to be designed such that the magnetic field they generate per unit current is maximal. This conflicts with the requirement of low resistance, which is important to keep the noise voltage small, and an optimal compromise must be found in practice between the two. It has been well known for

about two decades that the mass sensitivity (i.e., the signal/noise ratio per spin) of inductive detectors is roughly inversely proportional to the detector size. This can be rationalised by examining the normalised magnetic field and the radio frequency resistance of a particular detector geometry as a function of its overall dimensions. For example, the magnetic field generated by a single circular loop of diameter d made of a wire of thickness h is given approximately by $H/I = 1/(\pi d)$. If the geometry is scaled by a factor α, the H/I value therefore scales as α^{-1}. At typical NMR frequencies, the skin depth in Cu amounts only to a few μm. Therefore, as both the wire diameter and the loop diameter are scaled by the same factor α, the resistance of the structure remains roughly constant, as long as the wire diameter remains larger than the skin depth. As a result the signal to noise ratio is expected to scale roughly as $1/\alpha$. A similar argument can be made for solenoid coils. In practice, the observed scaling is weaker. Still, NMR detectors based on micro coils (i.e., with dimensions of tens to hundreds of μm) have been shown to provide very high mass sensitivities. This has formed the basis of hyphenated techniques, where upstream chromatographic separation is combined with downstream detection by an NMR system equipped with a micro detector.[9] Microfluidics is a rapidly expanding field of science and technology. The underlying idea is borrowed from micro electronics: to integrate complex functionality in a mostly two-dimensional layout, making use of efficient lithographic fabrication technologies. This lab-on-a-chip (LoC) approach has proven especially fruitful in enabling total analysis systems, which integrate sample preparation, chromatographic separation, and detection on single chip platform.[10] Since lithographic techniques allow the accurate reproduction of complex and very highly resolved features, microfluidic systems can be designed to mimic highly complex environments with great control and accuracy. This enables the culture of biological systems under artificial and highly controlled conditions, while closely mimicking the natural environment. This has become an invaluable tool for the study of differentiated cells, their development, and the interplay between different cell types. **REFS needed!!** NMR spectroscopy is uniquely suited to observe metabolic processes in live systems. It therefore has great potential as an observation tool in microfluidic culture assays. However, in spite of significant efforts, its use in the context of microfluidic devices is not yet widespread. There are a number of reasons for this. On the one hand, the planar geometry of microfluidic devices is not easily combined with common NMR detectors, which are typically designed for a cylindrical sample. Another limitation is the poor sensitivity of NMR, which is exacerbated by the small sample amounts typically available in microfluidic systems. As will become apparent in the following, micro stripline detectors are of particular interest in this context, since they inherently follow a planar geometry, and they can offer extremely high mass sensitivity. The first NMR probes based on a strip line geometry have been proposed in the context of magnetic resonance imaging. Their use for NMR spectroscopy at the microscope was first proposed by Maguire et al [11] in 2004. They integrated a stripline containing a small slot into a radio frequency resonator. The slot leads to current crowding, and consequently to a very large H/I value locally. This geometry provides excellent mass sensitivity, but the achieved spectral resolution was still relatively poor. A few years later, van Bentum and Kent-

gens and coworkers proposed a stripline detector based on a symmetric geometry with ground planes on either side of the strip line. By tapering the transition in the width of the strip line broadening of the resonance lines due to magnetic susceptibility artefacts could be largely reduced, [12] leading to excellent performance in terms of resolution. While these probes were operated in a flow mode, with fixed capillaries acting as sample holders, this geometry has recently been modified by Finch et al. to a transmission line probe based on two identical planar conductors, which can accommodate an exchangeable microfluidic chip. Looking into the future, strip line based detector geometries offer significant potential for further advances in miniaturisation. Their fabrication using lithographic techniques is straightforward, in contrast to intrinsically three-dimensional geometries such as solenoids, and there is no reason why they could not be successfully applied to detectors an order of magnitude or more smaller than the ones that have been demonstrated so far. Another exciting possibility is the use of stripline detectors in travelling wave mode, rather than as resonators carrying standing waves. Travelling wave NMR, which been demonstrated in the context of magnetic resonance imaging and (macroscopic) NMR spectroscopy, could have signifiant advantages at the micro scale, since it allows the spatial separation of the sample and the detection circuitry. The remainder of this chapter is organised as follows: first, some theoretical aspects of strip lines and strip-line based resonators are examined in section 2. Section 3 provides a chronological overview of the development of micro-NMR strip line and micro strip based detectors, and finally, section 4 discusses some of the recently demonstrated applications.

1.2
Striplines and Microslots: Basics and Theory

1.2.1
Definition of a stripline

The presence of conducting bodies imposes boundary conditions on the free propagation of electromagnetic waves. For an ideal conductor (an idealisation that certain metals, including Cu and Ag, approach quite closely), the electric field vector must stay perpendicular to the surface, while the magnetic field vector is required to stay parallel. Wave guides are long metallic structures of (usually) constant cross section. Electromagnetic waves of different types (modes) can propagate in the longitudinal direction in such structures. They are classified as transverse electric (TE) or transverse magnetic (TM) waves. In TE waves, the electric field has no component in the longitudinal direction, while the longitudinal magnetic field vanishes for TM waves. Both TE and TM wave modes can only propagate if the wave length is smaller than the lateral dimensions of the wave guide. This leads to a minimum frequency (often referred to as the cutoff frequency) for propagating modes. Also, the relationship between the wavelength and the frequency for TE and TM modes is non-linear, leading to dispersion. An additional type of propagating mode becomes possible if the walls of the wave guide are divided into several (at least 2) mutually insulated sections. In

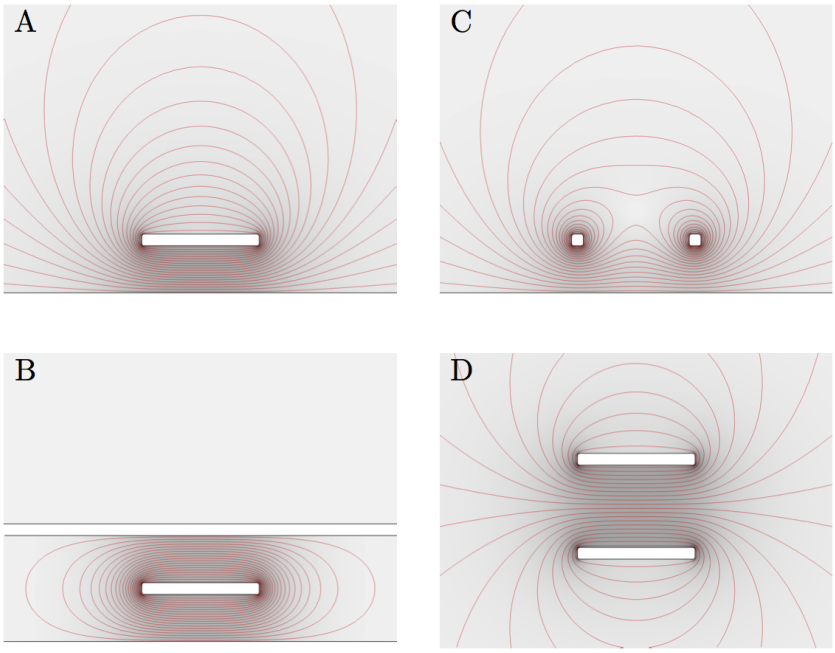

Figure 1.1 Cross section of some typical planar transmission line geometries, including magnetic field lines of the TEM mode. A: microstrip, B: stripline, C: microslot, D: parallel plate transmission line

this case, an oscillatory voltage can be sustained between the separate conductors. Under these conditions, a propagating modes exist *both* the electric and magnetic fields are transverse. Such TEM modes do not exhibit a cutoff frequency, and in general exhibit a linear relationship between wavelength and frequency. Frequencies of interest in magnetic resonance lie below 1.5 GHz. With usual dielectrics, this yields wave lengths of 20 cm or more. Therefore, TEM modes are commonly used in order to transport NMR signals, often in coaxial cables. This is different in electron paramagnetic resonance (EPR), where frequencies up to several hundred GHz occur. This requires the use of rectangular wave guides, in some cases with corrugated metalinterior surfaces. Fig. 1.1 shows some examples of common wave guide cross sections. Among these, the most familiar to NMR spectroscopists is that of the coaxial cable. Planar wave guide structures such as the microstrip (Fig XXXX b) and the stripline (Fig XXX c) are conveniently implemented on printed circuit boards, [13] and are very commonly used in the design of radio frequency and microwave circuits.

1.2.2
Characteristic Impedance and Transport Characteristics

For TEM modes, it is possible to attribute a current and a voltage amplitude to the travelling wave by integrating along the electric / magnetic field lines in the cross section. While the absolute voltage and current amplitudes depend on the level of wave excitation, their ratio (measured in Ohm) is a constant given purely by the cross section geometry, and the dielectric and magnetic properties of the insulating medium. This ratio is known as the characteristic impedance Z_0 of the wave guide. Coaxial cables are commonly designed for a characteristic impedance of 50 Ohm.

1.2.3
Theory of TEM Wave Modes

Maxwell's curl equations couple the magnetic field $\mathbf{H}$ and the electric field $\mathbf{E}$. If we assume a harmonic time evolution of the fields with angular frequency ω, they become

$$\nabla \times \mathbf{H} = j\omega\epsilon\mathbf{E} \tag{1.1}$$

$$\nabla \times \mathbf{E} = -j\omega\mu\mathbf{H} \tag{1.2}$$

where $j = \sqrt{-1}$ is the imaginary unit, and ϵ and μ represent the electric permittivity and magnetic permeability of the insulating medium, respectively. In order to analyse a TEM mode, we assume the axis of the transmission line to be aligned with the z direction. The two curl equations can be combined to the Helmholtz equation

$$(\nabla^2 + k^2)\mathbf{E} = 0, \tag{1.3}$$

where $k = \omega\sqrt{\mu\epsilon}$ is the wave number. If we assume a harmonic dependence in the z direction of the two transverse components, proportional to e^{-jkz}, it is easily shown that the transverse components must satisfy Laplace's equation, i.e.,

$$\left(\frac{\partial^2}{\partial x^2} + \frac{\partial^2}{\partial y^2}\right) E_{x,y} = 0. \tag{1.4}$$

A similar argument leads to the same result for the transverse magnetic field. The electric and magnetic field distribution in the cross section of a transmission line are therefore solutions to Laplace's equation. The fields satisfy the boundary conditions $\mathbf{E} \cdot \mathbf{n} = 0$ and $\mathbf{H} \times \mathbf{n} = 0$, where $\mathbf{n}$ is the surface normal. It is useful to note that the field distributions follow the same laws as in the case of completely static fields. In particular, this means that the field distribution inside a transmission line is *independent of the frequency*. Transmission lines are therefore inherently broadband devices, with no lower limit to the frequencies they can carry. In theory, there is no upper limit for the propagation of the TEM mode either; however, the excitation of TE and TM modes complicates the situation at very high frequencies. For this reason, coaxial transmission lines are only used up to frequencies of several tens of GHz. In addition, dielectric losses in commonly used insulators become intolerable at very high frequencies.

1.2.4 Modelling of TEM modes

Since the transverse electric and magnetic field distributions for TEM modes are solutions of the two-dimensional Laplace equation, they are easily computed for any geometry using a finite element or finite difference approach. It should be noted that the electric field is curl-free. Therefore, it can be represented as the gradient of an electrostatic potential $\phi(x, y)$, which also satisfies the Laplace equation. Computing the transverse field distribution therefore reduces to a simple Dirichlet problem, where fixed potential values must be attributed to the conductor surfaces:

$$\nabla^2\phi(x,y) = 0 \quad \text{on } B, \qquad \phi = V_{1,2,\ldots} \quad \text{on } \partial B_{1,2,\ldots}, \tag{1.5}$$

where B denotes the dielectric cross section, and $\partial B_{1,2,\ldots}$ represent the conductor surfaces, and $V_{1,2,\ldots}$ are the electrical surface potentials. The electric field of a propagating TEM mode is then given by

$$\mathbf{E} = e^{-\gamma z}\left(-\frac{\partial\phi}{\partial x}, -\frac{\partial\phi}{\partial x}, 0\right), \tag{1.6}$$

where $\gamma = \alpha + jk$ is the propagation constant, which describes both the oscillatory propagation of the wave in the z direction with wave number k and its gradual attenuation with decay constant α. [1)]

The magnetic field distribution is easily found using the the curl equations:

$$\mathbf{H} = e^{-\gamma z}\left(\frac{1}{\eta} - \frac{j\alpha}{\omega\mu}\right)\left(\frac{\partial\phi}{\partial x}, -\frac{\partial\phi}{\partial y}, 0\right), \tag{1.7}$$

where the characteristic impedance of the medium η is given by

$$\eta = \sqrt{\frac{\mu}{\epsilon}}. \tag{1.8}$$

Note that in the case of $\alpha = 0$, the magnetic and the electric field are *in phase*, whereas a positive attenuation constant $\alpha > 0$ leads to the magnetic field phase lagging behind the electric field. The time-averaged power transported by the TEM wave is given by real part the Poynting vector as

$$\Re(\mathbf{S}) = \frac{1}{2}\Re(\mathbf{E}\times\mathbf{H}^*) = p_t\,\hat{\mathbf{z}}, \tag{1.9}$$

where the cross-sectional density of power $p_t(x, y)$ is

$$p_t(x,y) = \frac{e^{-2\alpha z}}{2\eta}\left[\left(\frac{\partial\phi}{\partial x}\right)^2 + \left(\frac{\partial\phi}{\partial y}\right)^2\right]. \tag{1.10}$$

1) It should be noted that the foregoing treatment is only strictly exact in the limit $\alpha \ll k$. However, for transmission lines composed of polymer dielectrics and good conductors, this is almost always true to a good approximation.

The relative power loss per unit length is therefore given by

$$\frac{1}{p_t}\frac{\partial p_t}{\partial z} = -2\alpha. \tag{1.11}$$

At every cross section of the transmission line, it is possible to compute the electrical potential difference between the two conductors by a path integral between the condutcor surfaces

$$V(z) = \oint_1^2 \mathbf{E}(x,y,z)\cdot \mathrm{d}\mathbf{s}, \tag{1.12}$$

Similarly, the current flowing in the conductor can be obtained using Ampere's law

$$I(z) = \oint \mathbf{H}(x,y,z)\cdot \mathrm{d}\mathbf{s}, \tag{1.13}$$

where the integration path in this case is a closed loop around the conductor.

It is easily shown that the voltage and current thus obtained satisfy the equations

$$\frac{\mathrm{d}^2V}{\mathrm{d}z^2} = \gamma^2 V(z) \tag{1.14}$$

$$\frac{\mathrm{d}^2I}{\mathrm{d}z^2} = \gamma^2 I(z). \tag{1.15}$$

These equations are useful to describe the behaviour of transmission lines when integrated into electrical circuit networks. In general, they can be solved by a superposition of two waves travelling in opposite directions:

$$V(z) = V_0^+ e^{-\gamma z} + V_0^- e^{\gamma z} \tag{1.16}$$

$$I(z) = I_0^+ e^{-\gamma z} + I_0^- e^{\gamma z}. \tag{1.17}$$

The ratio

$$Z_0 = \frac{V_0^+}{I_0^+} = \frac{V_0^-}{I_0^-} \tag{1.18}$$

is known as the characteristic impedance of the transmission line. Its value depends entirely on the geometry of the transmission line cross section and on the the dielectric and magnetic properties of the insulator.

1.2.4.1 Losses in Transmission Lines

There are two main contributions to the power losses in a transmission line. On the one hand, there are dielectric losses due to the repeated polarisation and depolarisation of the insulating medium. These are proportional to the magnitude of the electric fields. The dielectric properties of most insulator materials are only very weakly frequency dependent; the dissipated power therefore tends to be proportional to the frequency. The dielectric dissipation of a material can be expressed by an imaginary component in its dielectric permittivity $\epsilon = \epsilon' + i\epsilon''$. Often, the loss tangent, defined as $\tan\delta = \epsilon''/\epsilon'$ is used in order to characterise the material. A second

(and, in the present context, often dominant) source of losses is the finite conductivity of the metallic surfaces. A plane electromagnetic wave impinging on an imperfect conductor penetrates into it only to a finite depth δ_s, known as the skin depth. This is because the tangential component of the magnetic field at the boundary induces in the surface a current which cancels the magnetic field deeper inside metal. Since this current is sustained against a finite ohmic resistance, it leads to heating and therefore to a loss of power from the electromagnetic wave. The dissipated power depends linearly on the magnetic field at the surface of the conductor. If the dimensions of the transmission line cross section are much larger than the skin depth, it is possible to express the average dissipated power per unit surface area as

$$P_\delta = \frac{1}{2}|H_\parallel|^2 R_s, \tag{1.19}$$

where R_s is the surface resistance of the metal. It depends on the material's conductance and the skin depth as

$$R_s = \frac{1}{\sigma\delta_s} = \sqrt{\frac{\omega\mu}{2\sigma}}, \tag{1.20}$$

where δ_s is the skin depth, and σ represents the conductivity. For pure Cu, $\sigma = 5.9 \cdot 10^7$S/m, which translates into a surface resistance of about 10 mΩ at 100 MHz, and about 35 mΩ at 1 GHz. The losses lead to a gradual attenuation of a travelling TEM mode, as reflected in the real part of the propagation constant γ. The conductive and dielectric losses are additive, such that we can write

$$\alpha = \alpha_d + \alpha_c. \tag{1.21}$$

In the following, we examine some planar transmission line geometries, and the relationship between their geometry, characteristic impedance, and attenuation constants.

1.2.5
Magnetic Fields and Losses in Transmission Lines, Striplines, Microstrips and Microslots

The magnetic and electric field distributions of the TEM mode in some planar transmission line geometries are shown in Fig XXX. Fig XXa shows a stripline, symmetrically bounded between two ground planes. The magnetic field lines encircle the central conductor, producing two areas of very high field homogeneity which can be used as sample locations for NMR spectroscopy. The stripline, shown in Fig. XXb, exhibits a similar field geometry. However, since there is only a single ground plane, the magnetic and electric fields penetrate into the free space above. This is less pronounced in practice than in the idealised computation shown here, since the dielectric constant of the insulator means that the electric field remains partially captured inside it. Nonetheless, the open geometry can lead to radiation losses, which must be kept to a minimum by external shielding. Fig. XXXc shows a microslot line. In

this case, there are two independent conductors, which can in principle carry different electrical potentials. This geometry is therefore capable of supporting more than one TEM mode. However, in the present context, only the common mode shown in Fig. XXXc is of interest. Compared to the similar microstrip geometry, the magnetic field is concentrated in the space immediate above the pair of conductors.

1.2.5.1 Transmission Line Resonators

- Dimensions and eigenfrequencies
- Q factor and sensitivity
-

1.3 Stripline NMR

References

1 Abragam, A. (1961) *The Principles of Nuclear Magnetism*, Oxford University Press.

2 Rabi, I., Zacharias, J., Millman, S., and Kusch, P. (1938) A new method of measuring nuclear magnetic moment. *Physical Review*, **53** (4), 318–318.

3 Bloch, F. (1946) Nuclear Induction. *Phys. Rev.*, **70** (7-8), 460–474.

4 Purcell, E.M., Torrey, H.C., and Pound, R.V. (1946) Resonance Absorption by Nuclear Magnetic Moments in a Solid. *Phys. Rev.*, **69** (1-2), 37–38.

5 Ernst, R.R. and Anderson, W.A. (1966) Application of Fourier Transform Spectroscopy to Magnetic Resonance. *Review of Scientific Instruments*, **37** (1), 93–102.

6 Bechinger, B. and Opella, S.J. (1991) Flat-coil probe for NMR spectroscopy of oriented membrane samples. *Journal of Magnetic Resonance (1969)*, **95** (3), 585–588.

7 Zhang, X., Ugurbil, K., and Chen, W. (2001) Microstrip RF surface coil design for extremely high-field MRI and spectroscopy. *Magn. Reson. Med.*, **46** (3), 443–450.

8 Hoult, D. and Richards, R. (1975) Critical Factors in the Design of Sensitive High Resolution Nuclear Magnetic Resonance Spectrometers. *Proceedings of the Royal Society of London. Series A, Mathematical and Physical Sciences*, **344** (1638), 311–340.

9 Webb, A. (2005) Nuclear magnetic resonance coupled microseparations. *Magn Reson Chem*, **43**, 688–696.

10 Manz, A., Graber, N., and WIDMER, H. (1990) Miniaturized Total Chemical-Analysis Systems - a Novel Concept for Chemical Sensing. *Sensor Actuat B-Chem*, **1**, 244–248.

11 Maguire, Y., Gershenfeld, N., and Chuang, I.L. (2009), Slitted and stubbed microstrips for high sensitivity, near-field electromagnetic detection of small samples and fields, US Patent Office.

12 Bart, J., Janssen, J.W.G., van Bentum, P.J.M., Kentgens, A.P.M., and Gardeniers, J.G.E. (2009) Optimization of stripline-based microfluidic chips for high-resolution NMR. *J. Magn. Reson*, **201** (2), 175–185.

13 Barret, R.M. (1955) Microwave Printed Circuits - A Historical Survey. *Microwave Theory and Techniques, IRE Transactions on*, **3** (2), 1–9.